Pergamon

Int. J. Solids Structures Vol. 31, No. 3, pp. 417–439, 1994

0020–7683/94 $6.00 + .00

GENERAL BEHAVIOR AND SHEAR CENTER LOCATION OF PRISMATIC ANISOTROPIC BEAMS VIA POWER SERIES

J. B. KOSMATKA
Department of Applied Mechanics and Engineering Science, University of California, San Diego, La Jolla, CA 92093, U.S.A.

(*Received* 27 *July* 1992; *in revised form* 2 *August* 1993)

Abstract—The behavior of a tip-loaded anisotropic cantilever beam with an arbitrary cross-section is studied using Saint-Venant's semi-inverse method along with a power series solution for the local in-plane and out-of-plane deformation warping functions. The power series coefficients are determined by solving a set of variationally derived linear algebraic equations. Using the resulting three-dimensional displacement solutions, the shear deformation associated with applied tip loads is investigated as well as the shear center location. Two different definitions of the shear center are presented for anisotropic beams by extending existing approaches developed for isotropic sections. Both of the extended definitions reveal the linear dependency of the shear center location on beam length. Numerical results are presented for three different cross-sections (ellipse, triangle, NACA-0012 airfoil) and two different materials (Al 6061-T6, off-angle high strength graphite/epoxy fibers).

INTRODUCTION

Closed-form solutions for Saint-Venant's problems (tip-loaded cantilever beam) exist for only a few simple isotropic homogeneous cross-section shapes (ellipse, rectangle, equilateral triangle) (Sokolnikoff, 1946) and one anisotropic homogeneous cross-section (ellipse) (Lekhnitskii, 1963). For general cross-section shapes, the local deformation functions of the cross-section cannot be determined exctly and thus approximate techniques must be used. One proven approach for approximately determining these local deformation in isotropic cross-sections (Herrmann, 1965; Mason and Herrmann, 1968) and anisotropic cross-sections (Kosmatka and Dong, 1991) involves the application of the finite element method. In this approach, the general anisotropic cross-section is discretized into triangular and/or quadrilateral subregions (elements) with in-plane and out-of-plane nodal variables that represent the local in-plane deformations and out-of-plane warping. But the finite element method requires a large number of elements for complex cross-sections, which will lead to a large set of linear algebraic equations (thousands of unknowns). Moreover, the calculated array of nodal deformations provides little insight into the deformation and warping distribution over the cross-section and thus one must resort to graphical finite element post-processing techniques to understand this distribution. An alternative approach, which has been used by Mindlin (1975) for the solution of Saint-Venant's isotropic torsion problem and by Kosmatka (1992) for the isotropic flexure problem, involves assuming a double power series for each of the local in-plane deformations and the out-of-plane warping. The power series coefficients are determined by solving a set of linear algebraic equations, where the number of equations is equal to the number of unknown coefficients. Thus, the problem size is independent of the cross-section complexity, and only dependent on the number of terms in the power series.

The objective of this paper is to develop a method for studying the behavior of tip-loaded anisotropic beams with general cross-sections using Saint-Venant's semi-inverse method, where the local deformations of the cross-section are expressed as a double power series in terms of the cross-section coordinates. The coefficients associated with the power series terms are determined by solving a set of variationally derived linear algebraic equations, where the number of equations is equal to the number of unknown coefficients. For complex cross-sections, the calculated coefficients represent a "best-fit approximation" to the exact warping function which may be an infinite series of transcendental functions. To aid in the evaluation of the power series weighted area integrals, the cross-section is

discretized into a series of triangular subregions, where the integration in each subregion is evaluated exactly using Gaussian Quadrature formulae for triangles (Dunavant, 1985). The triangle aspect ratio is not critical, as opposed to the finite element method, since the power series is a global cross-section function and not a local element function.

Numerical results are presented for three different cross-sections (ellipse, triangle, NACA-0012) and two different materials (Al 6061-T6, off-angle high-strength graphite/epoxy fibers) to first validate the approach, second prove convergence of warping related cross-section parameters (torison constant, shear center location, shear deformation), third present important behavioral data not currently found in the literature and fourth investigate the sensitivity of the shear center location with cross-section shape, beam length and material definition. The solution procedure and results from the current study will be of interest to developers of one-dimensional theories for general anisotropic prismatic beams, who can use the current general Saint-Venant displacement, stress, and local deformation solutions to: (1) provide a frame-work for insuring that the requisite "extension-bend-twist-shear" coupling effects are properly included, (2) determine all of the required one-dimensional local deformation (warping) dependent cross-section constants (for example torsion stiffness, shear stiffness, coupling stiffnesses, etc.), (3) define the limits of applicability of their proposed theories. Moreover, the numerical results on shear deformation and the line of shear centers provides important physical insight into the complex behavior of generally anisotropic prismatic beams and the profound tailorability that is possible using advanced composite materials in wing and blade designs.

THEORETICAL BACKGROUND

We begin by considering a cantilevered prismatic beam of length L with an arbitrary cross-section of area A composed of a homogeneous, rectilinearly anisotropic material. A rectangular Cartesian coordinate system x, y, z, with corresponding displacements u, v, w, is established with the origin at the centroid of the root end and the x, y axes coincide with the cross-section principal axes (see Fig. 1). The constitutive relations for the material are given by:

$$\{\sigma\} = [C]\{\varepsilon\},$$
$$\{\varepsilon\} = [S]\{\sigma\},$$
$$[C] = [S]^{-1}, \tag{1a–c}$$

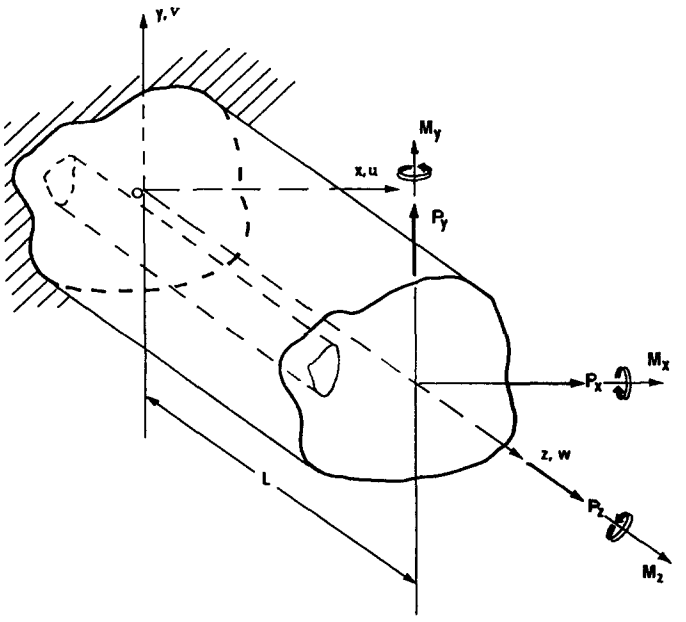

Fig. 1. Anisotropic cantilever beam.

where $[C]$ and $[S]$ are fully populated symmetric matrices with 21 distinct elements and the stress and strain arrays are given as:

$$\{\sigma\} = \{\sigma_{xx}, \sigma_{yy}, \sigma_{zz}, \tau_{yz}, \tau_{xz}, \tau_{xy}\},$$
$$\{\varepsilon\} = \{\varepsilon_{xx}, \varepsilon_{yy}, \varepsilon_{zz}, \gamma_{yz}, \gamma_{xz}, \gamma_{xy}\}. \tag{1d,e}$$

At the root end, the beam is fully fixed. Within the framework of the Saint-Venant problems, this condition cannot be described on a point-wise basis and the equivalent statement at the centroid ($x = y = z = 0$) can be used:

$$u = v = w = 0,$$
$$\frac{\partial u}{\partial z} = \frac{\partial v}{\partial z} = \frac{\partial v}{\partial x} - \frac{\partial u}{\partial y} = 0. \tag{2a–f}$$

This root fixity condition is not unique and other possible root fixity conditions can also be easily considered. For example, Mason and Herrmann (1968) studied the flexure behavior of an isotropic beam by setting to zero the average root displacements and rotations.

At the free end, tractions are applied which reduce to an equivalent force P and moment M with respect to the cross-section centroid. The force P and moment M can be decomposed into flexure components, P_x and P_y, an extensional component, P_z, bending moments, M_x and M_y, and a torsion moment, M_z. As a result of the applied tip loads, five of the stresses are independent of z and the sixth stress σ_{zz} has flexure components which vary linearly with z:

$$\sigma_{zz} = \left\{\frac{P_x}{I_{yy}} x + \frac{P_y}{I_{xx}} y\right\} z + \sigma_{zz}^0(x, y), \tag{3}$$

where I_{xx} and I_{yy} are the area moments of inertia about the x and y axes, respectively, and σ_{zz}^0 is associated with extension, bending and torsion. Introducing these assumptions into the stress equilibrium equations and integrating yields the following displacement and strain components [see Kosmatka (1986) and Kosmatka and Dong (1991) for further details]:

$$u = -\frac{P_x}{2EI_{yy}}\left\{\frac{z^2}{3}(z-3L) - \frac{\nu_4}{2} yz(z-2L) + \{\nu_1 x^2 - \nu_2 y^2\}(z-L)\right\} + \frac{1}{2EI_{yy}}\left\{M_y + \frac{\nu_4}{2} M_z\right\} z^2$$
$$-\theta yz - \frac{P_y}{2EI_{xx}}\left\{\{2\nu_1 x + \nu_6 y\} y(z-L) + \frac{\nu_5}{2} yz(z-2L)\right\} + \psi_x(x, y), \tag{4a}$$

$$v = -\frac{P_y}{2EI_{xx}}\left\{\frac{z^2}{3}(z-3L) - \frac{\nu_5}{2} xz(z-2L) + \{\nu_2 y^2 - \nu_1 x^2\}(z-L)\right\} - \frac{1}{2EI_{xx}}\left\{M_x + \frac{\nu_5}{2} M_z\right\} z^2$$
$$+\theta xz - \frac{P_x}{2EI_{yy}}\left\{\{\nu_6 x + 2\nu_2 y\} x(z-L) + \frac{\nu_4}{2} xz(z-2L)\right\} + \psi_y(x, y), \tag{4b}$$

$$w = -\frac{P_x}{2EI_{yy}}\{\{\nu_5 x + \nu_4 y\} x(z-L) - xz(z-2L)\} - \frac{1}{EI_{yy}}\left\{M_y + \frac{\nu_4}{2} M_z\right\} xz$$
$$+ \frac{1}{EI_{xx}}\left\{M_x + \frac{\nu_5}{2} M_z\right\} yz - \frac{P_y}{2EI_{xx}}\{\{\nu_5 x + \nu_4 y\} y(z-L) - yz(z-2L)\}$$
$$-\frac{1}{EA}\left\{\frac{\nu_5}{2} P_x + \frac{\nu_4}{2} P_y - P_z\right\} z + \psi_z(x, y) \tag{4c}$$

and

$$\varepsilon_{xx} = -\frac{P_x v_1}{EI_{yy}} x(z-L) - \frac{P_y v_1}{EI_{xx}} y(z-L) + \frac{\partial \psi_x}{\partial x}, \tag{4d}$$

$$\varepsilon_{yy} = -\frac{P_x v_2}{EI_{yy}} x(z-L) - \frac{P_y v_2}{EI_{xx}} y(z-L) + \frac{\partial \psi_y}{\partial y}, \tag{4e}$$

$$\varepsilon_{zz} = -\frac{P_x}{2EI_{yy}} \{v_5 x + v_4 y + 2(L-z)\} x - \frac{P_y}{2EI_{xx}} \{v_5 x + v_4 y + 2(L-z)\} y + \frac{1}{EI_{xx}} \left\{M_x + \frac{v_5}{2} M_z\right\} y - \frac{1}{EI_{yy}} \left\{M_y + \frac{v_4}{2} M_z\right\} x - \frac{1}{2EA} \{v_5 P_x + v_4 P_y - 2P_z\}, \tag{4f}$$

$$\gamma_{yz} = -\frac{P_x}{EI_{yy}} \left\{\frac{v_6}{2} x + v_2 y + v_4 (z-L)\right\} x + \frac{P_y}{2EI_{xx}} \{v_1 x^2 - v_2 y^2 - 2v_4 y(z-L)\} + \theta x + \frac{\partial \psi_z}{\partial y}, \tag{4g}$$

$$\gamma_{xz} = -\frac{P_y}{EI_{xx}} \left\{v_1 x + \frac{v_6}{2} y + v_5 (z-L)\right\} y - \frac{P_x}{2EI_{yy}} \{v_1 x^2 - v_2 y^2 + 2v_5 x(z-L)\} - \theta y + \frac{\partial \psi_z}{\partial x}, \tag{4h}$$

$$\gamma_{xy} = -\frac{P_x v_6}{EI_{yy}} x(z-L) - \frac{P_y v_6}{EI_{xx}} y(z-L) + \frac{\partial \psi_x}{\partial y} + \frac{\partial \psi_y}{\partial x}, \tag{4i}$$

where A is the cross-section area, θ is the twist rate of the beam about the centroidal axis (z), that is a function of the three force components (P_x, P_y, P_z) and the three moment components (M_x, M_y, M_z), E $(= 1/S_{33})$ is commonly called Young's modulus, and v_i are cross-coupling coefficients defined as:

$$v_i = -\frac{S_{i3}}{S_{33}}. \tag{4j}$$

Here v_1 and v_2, are the usual Poisson coefficients, and v_4, v_5 and v_6, express the three-dimensional extension-shear coupling that can occur in a completely anisotropic body. The remaining functions (ψ_x, ψ_y, ψ_z) represent local cross-section x, y dependent deformations and are unique for each cross-section shape and material configuration, and are linearly proportional to the six applied loads. In the current development, the local cross-section deformations are first calculated in terms of the six applied loads and the twist rate, then a linear relation is developed that expresses the twist rate in terms of the six applied loads, and finally this relation is used to express the local deformations, stresses, and displacements in terms of only the six applied loads. Writing the local deformations in terms of the six applied loads and the twist rate [see Kosmatka and Dong (1991)]

$$(\psi_x, \psi_y, \psi_z) = \sum_{i=1}^{7} (\psi_{x(i)}, \psi_{y(i)}, \psi_{z(i)}) Q_i, \tag{4k}$$

where Q_i are the components of

$$\{Q\}^{\mathrm{T}} = \{P_x, P_y, P_z, M_x, M_y, M_z, \theta\}. \tag{4l}$$

The "unit" local cross-section deformations $(\psi_{x(i)}, \psi_{y(i)}, \psi_{z(i)})$ are assumed to have the form of a power series:

$$\psi_{x(i)} = \sum_{m=0}^{\infty} \sum_{n=0}^{\infty} a_{mn(i)} x^m y^n,$$

$$\psi_{y(i)} = \sum_{m=0}^{\infty} \sum_{n=0}^{\infty} b_{mn(i)} x^m y^n,$$

$$\psi_{z(i)} = \sum_{m=0}^{\infty} \sum_{n=0}^{\infty} c_{mn(i)} x^m y^n, \tag{5a–c}$$

where $(a_{mn(i)}, b_{mn(i)}, c_{mn(i)})$ are unknown coefficients that depend upon the cross-section shape, material properties and load-type Q_i, and the subscripts m and n correspond to the order of x and y, respectively. The four rigid body motions of the cross-section (three translations, rotation about the z-axis) for each of the seven cases are constrained by setting $(a_{00} = b_{00} = c_{00} = 0)$ and requiring that $(a_{01} = b_{10})$. Assuming that the series is finite, eqns (4k) and (5a–c) are combined to form:

$$\{\psi\} = [H][\Psi]\{Q\}, \tag{6a}$$

where

$$\{\psi\}^{\mathrm{T}} = \{\psi_x, \psi_y, \psi_z\},$$

$$[H] = \begin{bmatrix} [N(x,y)] & 0 & 0 \\ 0 & [N(x,y)] & 0 \\ 0 & 0 & [N(x,y)] \end{bmatrix}, \tag{6b, c}$$

and $[\Psi]$ is comprised of seven columns of unknown coefficients that have the form:

$$\{\psi_{(i)}\}^{\mathrm{T}} = \{\{a_{(i)}\}^{\mathrm{T}}, \{b_{(i)}\}^{\mathrm{T}}, \{c_{(i)}\}^{\mathrm{T}}\}, \quad i = 1, \ldots, 7. \tag{6d}$$

For example, if a cubic polynomial was selected, then based upon Pascal's triangle, $[N(x,y)]$ has 10 terms:

$$[N(x,y)] = \{1, x, y, x^2, xy, y^2, x^3, x^2y, xy^2, y^3\}, \tag{7a}$$

and $\{a_{(i)}\}$, $\{b_{(i)}\}$ and $\{c_{(i)}\}$ for the ith column of $[\Psi]$ has the form:

$$\{a_{(i)}\}^{\mathrm{T}} = \{a_{00(i)}, a_{10(i)}, a_{01(i)}, a_{20(i)}, a_{11(i)}, a_{02(i)}, a_{30(i)}, a_{21(i)}, a_{12(i)}, a_{03(i)}\},$$

$$\{b_{(i)}\}^{\mathrm{T}} = \{b_{00(i)}, b_{10(i)}, b_{01(i)}, b_{20(i)}, b_{11(i)}, b_{02(i)}, b_{30(i)}, b_{21(i)}, b_{12(i)}, b_{03(i)}\},$$

$$\{c_{(i)}\}^{\mathrm{T}} = \{c_{00(i)}, c_{10(i)}, c_{01(i)}, c_{20(i)}, c_{11(i)}, c_{02(i)}, c_{30(i)}, c_{21(i)}, c_{12(i)}, c_{03(i)}\}, \tag{7b–d}$$

and the aforementioned three rigid body translations and one rigid body rotation are constrained using standard finite procedures after the cross-section model is fully assembled.

The strain array $\{\varepsilon\}$ of eqn (1e) can be obtained in terms of the matrix of unknown coefficients $[\Psi]$, the applied forces and moments, and the centroidal twist rate by substituting eqn (6a) into eqns (4d–i):

$$\{\varepsilon\} = \{[B][\Psi] + [\overline{F_{\mathrm{C}}}]\}\{Q\}, \tag{8a}$$

where

$$[B]^{\mathrm{T}} = \begin{bmatrix} \dfrac{\partial[N(x,y)]}{\partial x} & 0 & 0 & 0 & 0 & \dfrac{\partial[N(x,y)]}{\partial y} \\ 0 & \dfrac{\partial[N(x,y)]}{\partial y} & 0 & 0 & 0 & \dfrac{\partial[N(x,y)]}{\partial x} \\ 0 & 0 & 0 & \dfrac{\partial[N(x,y)]}{\partial y} & \dfrac{\partial[N(x,y)]}{\partial x} & 0 \end{bmatrix} \tag{8b}$$

and $[\overline{F_{\mathrm{C}}}]$ is defined in the Appendix.

The magnitude of the unknown coefficients in $[\Psi]$ can be determined by applying the principle of minimum potential energy:

$$\delta\Pi = \delta U - \delta W_{\mathrm{e}} = 0, \tag{9a}$$

where δU is the variation of the strain energy;

$$\delta U = \int_0^L \int_A \{\delta\varepsilon\}^{\mathrm{T}}[C]\{\varepsilon\}\,\mathrm{d}A\,\mathrm{d}z, \tag{9b}$$

and δW_{e} is the variation of the work of external forces that results from the applied tractions on the beam ends:

$$\delta W_{\mathrm{e}} = \int_A \{\tau_{xz}\delta\psi_x + \tau_{yz}\delta\psi_y + \sigma_{zz}\delta\psi_z\}|_{(z=L)}\,\mathrm{d}A - \int_A \{\tau_{xz}\delta\psi_x + \tau_{yz}\delta\psi_y + \sigma_{zz}\delta\psi_z\}|_{(z=0)}\,\mathrm{d}A, \tag{9c}$$

which reduces to (Kosmatka and Dong, 1991):

$$\delta W_{\mathrm{e}} = \frac{P_x L}{I_{yy}} \int_A x\delta\psi_z\,\mathrm{d}A + \frac{P_y L}{I_{xx}} \int_A y\delta\psi_z\,\mathrm{d}A. \tag{9d}$$

A set of linear algebraic equations for determining the seven "unit" unknown deformation coefficients is obtained by substituting (8a), (9b) and (9d) into (9a), integrating over the beam volume, and taking the variation with respect to the unknown coefficients:

$$[K][\Psi] = [[F_{\mathrm{W}}] - [F_{\mathrm{C}}]], \tag{10a}$$

where

$$[K] = L\int_A [B]^{\mathrm{T}}[C][B]\,\mathrm{d}A, \tag{10b}$$

$$[F_{\mathrm{W}}] = L\begin{bmatrix} 0 & 0 & 0 & 0 & 0 & 0 & 0 \\ 0 & 0 & 0 & 0 & 0 & 0 & 0 \\ \dfrac{1}{I_{yy}}\displaystyle\int_A x[N(x,y)]\,\mathrm{d}A & \dfrac{1}{I_{xx}}\displaystyle\int_A y[N(x,y)]\,\mathrm{d}A & 0 & 0 & 0 & 0 & 0 \end{bmatrix}, \tag{10c}$$

and

$$[F_{\mathrm{C}}] = L\int_A [B]^{\mathrm{T}}[C][\overline{\overline{F_{\mathrm{C}}}}]\,\mathrm{d}A, \tag{10d}$$

with $[\overline{\overline{F_{\mathrm{C}}}}]$ also being defined in the Appendix. The final form of the local cross-section deformations [eqn (4k)] is determined by solving eqn (10a) for $[\Psi]$ and substituting the results into eqn (6a). Similarly, the stress components [eqn (1d)] can be written in terms of $\{Q\}$, using eqns (1a) and (8a), as

$$\{\sigma\} = [\bar{\sigma}]\{Q\}, \tag{11a}$$

where

$$[\bar{\sigma}] = [C][[B][\Psi]+[\overline{F_C}]]. \tag{11b}$$

The centroidal twist rate $\theta(Q_7)$ can now be determined in terms of the three applied forces and moments by substituting the fourth (τ_{yz}) and fifth (τ_{xz}) rows of eqn (11a) into the cross-section torsion moment equilibrium equation:

$$M_z = \int_A x\tau_{yz} - y\tau_{xz}\,\mathrm{d}A, \tag{12a}$$

integrating, and rearranging to get:

$$\theta = a_1P_x + a_2P_y + a_3P_z + a_4M_x + a_5M_y + a_6M_z, \tag{12b}$$

where

$$a_k = -\frac{\overline{a_k}}{\overline{a_7}}, \quad (k = 1, \ldots, 5), \tag{12c}$$

$$a_6 = \frac{1-\overline{a_6}}{\overline{a_7}} \tag{12d}$$

and

$$\overline{a_k} = \int_A \{x(\bar{\sigma}_{4k}) - y(\bar{\sigma}_{5k})\}\,\mathrm{d}A, \quad (k = 1, \ldots, 7). \tag{12e}$$

The i and j subscripts σ_{ij} in eqn (12e) correspond to the row and column positions in $[\bar{\sigma}]$ [eqn (11b)]. The coefficients a_1–a_6 are all independent of the beam-length because from the original assumptions, the shear stress distribution is only a function of the cross-section coordinates x and y. Moreover, the torsion stiffness is commonly defined as: $GJ = 1/a_6$ [see Kosmatka and Dong (1991)].

Lastly, the local deformations and the stress array can be expressed in terms of only the three applied forces and moments by combining eqn (12b) with eqns (6a), (8a) and (11a):

$$\begin{Bmatrix} \psi_x \\ \psi_y \\ \psi_z \end{Bmatrix} = [H][\Psi][T]\{Q^*\}, \tag{13a}$$

$$\{\varepsilon\} = [[B][\Psi]+[\overline{F_C}]][T]\{Q^*\}, \tag{13b}$$

$$\{\sigma\} = [C][[B][\Psi]+[\overline{F_C}]][T]\{Q^*\}, \tag{13c}$$

where

$$[T] \begin{bmatrix} 1 & 0 & 0 & 0 & 0 & 0 \\ 0 & 1 & 0 & 0 & 0 & 0 \\ 0 & 0 & 1 & 0 & 0 & 0 \\ 0 & 0 & 0 & 1 & 0 & 0 \\ 0 & 0 & 0 & 0 & 1 & 0 \\ 0 & 0 & 0 & 0 & 0 & 1 \\ a_1 & a_2 & a_3 & a_4 & a_5 & a_6 \end{bmatrix} \tag{13d}$$

and

$$\{Q^*\}^{\mathrm{T}} = \{P_x, P_y, P_z, M_x, M_y, M_z\}. \tag{13e}$$

BEHAVIOR OF AN ANISOTROPIC BEAM

The general behavior of a cantilever anisotropic beam having an arbitrary cross-section can now be studied using the displacement (4a–c) and stress distributions (13b) along with the calculated twist rate (12b) and the cross-section deformations (13a). In a previous paper (Kosmatka and Dong, 1991), a detailed discussion was presented covering the extension, bending, torsion and flexure behavior of anisotropic cantilever prismatic beams based upon Saint-Venant solutions. In the current paper, we will focus our discussions on two topics: shear deformation and further issues concerning the shear center location.

Shear deformation

An examination of the transverse displacements (u, v), from eqns (4a, b), reveals that applying either a bending moment (M_x, M_y) or a flexure force (P_x, P_y) will produce centroidal tip components $(x = y = 0, z = L)$ that agree with the standard (isotropic) strength of material solutions

$$u(x = y = 0, z = L) = \frac{P_x L^3}{3EI_{yy}} + \frac{M_y L^2}{2EI_{yy}}, \qquad v(x = y = 0, z = L) = \frac{P_y L^3}{3EI_{xx}} - \frac{M_x L^2}{2EI_{xx}}, \tag{14a, b}$$

and applying an extension force (P_z) will produce only an axial component (w). But the transverse components associated with shear deformation are not included in eqns (4a–c) because the fixed root boundary was defined by setting the deformed centroidal axis slope to zero $(\partial u/\partial z = \partial v/\partial z = 0)$. These additional transverse components can be included by simply rotating the deformed beam so that the slope of the deformed cross-section at the centroid $(x = y = 0)$ is coincident with the x–y plane, and thus the deformed centroidal axis will have a nonzero slope at the origin. These rotation angles are equal to the shear strains $(\gamma_{xz}, \gamma_{yz})$ at the centroid of the beam root and can be found by evaluating the fourth and fifth equations of eqn (13b) at $(x = y = z = 0)$. For example the rotation angle, about the y-axis, associated with shear deformation in the x–z plane is equal [from eqns (4h), (5c) and (13a)] to:

$$\gamma_{xz_{(0)}} = \gamma_{xz}|_{x=y=0} = \left.\frac{\partial \psi_z}{\partial x}\right|_{x=y=0} = \sum_{i=1}^{6} (c_{10(i)} + a_i c_{10(7)}) Q_i^*. \tag{15}$$

Similarly the rotation angle, about the $-x$-axis, associated with shear deformation in the y–z plane is equal to:

$$\gamma_{yz_{(0)}} = \left.\frac{\partial \psi_z}{\partial y}\right|_{x=y=0} = \sum_{i=1}^{6} (c_{01(i)} + a_i c_{01(7)}) Q_i^*. \tag{16}$$

The final forms of the displacement components including shear deformation are

$$u = -\frac{P_x}{2EI_{yy}}\left\{\frac{z^2}{3}(z-3L) - \frac{v_4}{2} yz(z-2L) + \{v_1 x^2 - v_2 y^2\}(z-L)\right\} + \frac{1}{2EI_{yy}}\left\{M_y + \frac{v_4}{2} M_z\right\} z^2$$
$$-\theta yz - \frac{P_y}{2EI_{xx}}\left\{\{2v_1 x + v_6 y\} y(z-L) + \frac{v_5}{2} yz(z-2L)\right\} + \gamma_{xz_{(0)}} z + \psi_x(x, y), \tag{17a}$$

$$v = -\frac{P_y}{2EI_{xx}}\left\{\frac{z^2}{3}(z-3L) - \frac{v_5}{2} xz(z-2L) + \{v_2 y^2 - v_1 x^2\}(z-L)\right\} - \frac{1}{2EI_{xx}}\left\{M_x + \frac{v_5}{2} M_z\right\} z^2$$
$$+\theta xz - \frac{P_x}{2EI_{yy}}\left\{\{v_6 x + 2v_2 y\} x(z-L) + \frac{v_4}{2} xz(z-2L)\right\} + \gamma_{yz_{(0)}} z + \psi_y(x, y), \tag{17b}$$

$$w = -\frac{P_x}{2EI_{yy}}\{\{v_5x+v_4y\}x(z-L)-xz(z-2L)\}-\frac{1}{EI_{yy}}\left\{M_y+\frac{v_4}{2}M_z\right\}xz$$

$$+\frac{1}{EI_{xx}}\left\{M_x+\frac{v_5}{2}M_z\right\}yz-\frac{P_y}{2EI_{xx}}\{\{v_5x+v_4y\}y(z-L)-yz(z-2L)\}$$

$$-\frac{1}{EA}\left\{\frac{v_5}{2}P_x+\frac{v_4}{2}P_y-P_z\right\}z-\gamma_{xz_{(0)}}x-\gamma_{yz_{(0)}}y+\psi_z(x,y), \quad (17c)$$

where $\theta, \psi_x, \psi_y, \psi_z, \gamma_{xz_{(0)}}$ and $\gamma_{yz_{(0)}}$ are defined in eqns (12b), (13a), (15) and (16), respectively.

Shear center location. Line of shear centers

For prismatic cantilever beams that exhibit less than generally anisotropic behavior ($v_4, v_5 = 0$), the shear center is a property of the cross-section and independent of beam-length (the line of shear centers is parallel to the centroidal axis). For this class of materials, a classic definition has been presented for locating the shear center (Griffith and Taylor, 1917) as "the load point that produces a zero mean value cross-section twist rate (i.e., zero twist rate about the centroidal axis)." Attempting to extend this definition to a beam composed of a generally anisotropic material ($v_4, v_5 \neq 0$) leads to a shear center location that is a function of the cross-section shape, material definition and is *linearly* dependent upon beam-length (Kosmatka and Dong, 1991). Thus, the line of shear centers for a generally anisotropic beam is straight, but it is not parallel to the centroidal axis.

We can study this phenomena by calculating the micromolar twist rate for a particle in the beam:

$$\frac{\partial\omega_z}{\partial z}=\frac{1}{2}\left(\frac{\partial\gamma_{yz}}{\partial x}-\frac{\partial\gamma_{xz}}{\partial y}\right)=\theta-\frac{P_x}{2EI_{yy}}\{v_6x+2v_2y+v_4(z-L)\}$$

$$+\frac{P_y}{2EI_{xx}}\{2v_1x+v_6y+v_5(z-L)\}, \quad (18)$$

where the z-dependent terms are associated with anisotropic "bend–twist" coupling as a result of applied flexure. This z-dependency of the twist rate with applied flexure was observed by Libove (1988) in his study of single-cell thin-walled anisotropic beams. The micromolar twist rate about the centroidal axis ($x = y = 0$), to be consistent with the work of (Griffith and Taylor, 1917), is:

$$\frac{\partial\omega_z}{\partial z}=\theta-\frac{P_xv_4}{2EI_{yy}}(z-L)+\frac{P_yv_5}{2EI_{xx}}(z-L). \quad (19)$$

Next, we apply a general tip flxural force (P_{xs}, P_{ys}) through the unknown shear center location (x_s, y_s), where the equivalent centroidal forces and moments are defined as

$$P_x = P_{xs}, \qquad P_y = P_{ys}, \qquad M_z = P_{ys}x_s - P_{xs}y_s. \quad (20a\text{–}c)$$

Substituting eqns (20a–c) and (12) into eqn (19) results in

$$\frac{\partial\omega_z}{\partial z}=P_{xs}\left(a_1-a_6y_s-\frac{v_4}{2EI_{yy}}(z-L)\right)+P_{ys}\left(a_2+a_6x_s+\frac{v_5}{2EI_{xx}}(z-L)\right). \quad (21)$$

Since the micromolar twist rate $(\partial\omega_z/\partial z)$ varies linearly with (z) for a generally anisotropic

beam, it is not possible to locate the shear center so that the twist rate about the centroidal axis is zero independent of beam axial position. Thus the Griffith and Taylor definition cannot be implemented if ($v_4, v_5 \neq 0$). Instead, we recognize that since the twist rate varies linearly with z, then the micromolar twist (ω_z) will vary quadratically with (z). Thus, the best that can be achieved is to "locate the shear center (x_s, y_s) so that there is zero micromolar twist at the beam root ($z = 0$) and zero twist in the cross-section plane that contains the applied load (for a tip load, $z = L$)." This is accomplished by setting

$$\int_0^L \frac{\partial \omega_z}{\partial z} \, dz = 0. \tag{22}$$

This is analogous to setting the average micromolar twist rate to zero over the beam length, which was proposed by Libove (1988) for single-cell thin-wall anisotropic sections. Substituting eqn (21) into eqn (22), carrying out the integration, and solving, produces the shear center location for the beam tip cross-section ($z = L$) that is independent of the magnitude of the applied loads:

$$x_s(z = L) = x_{sL} = -\frac{1}{a_6}\left\{a_2 - \frac{v_5 L}{4EI_{xx}}\right\}, \qquad y_s(z = L) = y_{sL} = \frac{1}{a_6}\left\{a_1 + \frac{v_4 L}{4EI_{yy}}\right\}. \tag{23a, b}$$

The shear center location at the root of a generally anisotropic beam (or a very short anisotropic beam ($L \approx 0$)) is equal to the classic Griffith/Taylor definition for an isotropic cross-section ($x_{s0} = -a_2/a_6$, $y_{s0} = a_1/a_6$). The shear center location in the beam-tip cross-section [eqn (23a, b)] is composed of two terms; one which is independent of the beam-length (i.e. the classic Griffith/Taylor definition) and one which is linearly proportional to the beam-length, the material properties (v_4, v_5), and the ratio of the torsion stiffness to the bending stiffness [$1/(a_6 EI_{xx})$, $1/(a_6 EI_{yy})$].

An alternate shear center definition has been presented by Reissner (1989, 1991) using thin-plate theory so that "the application of an applied flexture force will produce zero twist about the calculated line of shear centers" and thus insure that the shear center is coincident with the center of twist. Recently, Kosmatka (1992) applied Reissner's definition to the Saint-Venant flexure and torsion problems of a general prismatic isotropic beam and developed a linear relationship for calculating the Reissner shear center location (x_s^*, y_s^*) in terms of the classic Griffith–Taylor location (x_{s0}, y_{s0}):

$$x_s^* = \frac{x_{s0}}{1 + v\dfrac{GJ}{EI_{xx}}}, \qquad y_s^* = \frac{y_{s0}}{1 + v\dfrac{GJ}{EI_{yy}}}, \tag{24a, b}$$

where ($GJ = 1/a_6$). It was shown for isotropic beams that the two locations are very close if the cross-section is moderately thick, but if the cross-section is very thin (i.e. thin triangular or airfoil section), so that (GJ/EI) is large, then the difference in the two locations can be substantial with the Reissner shear center location being much closer to the centroid.

Now to apply the Reissner definition to a generally anisotropic beam with an arbitrary cross-section, we again apply a general flexure force (P_{xs}, P_{ys}) through an unknown shear center location (x_{sL}^*, y_{sL}^*) in the tip ($z = L$) cross-section, where the equivalent centroidal forces and moments are given in eqns (20a–c) and the micromolar twist rate about the unknown shear center location is determined by substituting eqns (20a–c) and (12b) into eqn (18):

$$\frac{\partial \omega_z}{\partial z} = P_{xs}\left(a_1 - a_6 y^*_{sL} - \frac{1}{2EI_{yy}}\{v_6 x^*_{sL} + 2v_2 y^*_{sL} + v_4(z-L)\}\right)$$
$$+ P_{ys}\left(a_2 + a_6 x^*_{sL} + \frac{1}{2EI_{xx}}\{2v_1 x^*_{sL} + v_6 y^*_{sL} + v_5(z-L)\}\right). \quad (25)$$

Once again, the micromolar twist rate $(\partial\omega_z/\partial z)$ varies linearly with (z), and thus the best that can be attained for an anisotropic beam is to locate the shear center so that the micromolar twist (ω_z) is zero at the beam root $(z = 0)$ and beam tip (load plane, $z = L$) and varies quadratically between the root and tip. Substituting eqn (25) into eqn (22) and carrying out the integration over the beam-length, results in two coupled linear algebraic equations that are used to solve for the shear center location in the beam-tip cross-section:

$$\begin{bmatrix} a_6 + \dfrac{v_1}{EI_{xx}} & \dfrac{v_6}{2EI_{xx}} \\ \dfrac{v_6}{2EI_{yy}} & a_6 + \dfrac{v_2}{EI_{yy}} \end{bmatrix} \begin{Bmatrix} x^*_{sL} \\ y^*_{sL} \end{Bmatrix} = \begin{Bmatrix} -a_2 + \dfrac{v_5 L}{4EI_{xx}} \\ a_1 + \dfrac{v_4 L}{4EI_{yy}} \end{Bmatrix}. \quad (26)$$

An examination of the above equation reveals that: (1) this shear center location for anisotropic beams will identically reduce to the Reissner definition of eqn (24) for isotropic materials $(v_4, v_5, v_6 = 0)$; (2) the form of the length-dependency effects is identical to that of eqn (23), which was developed by extending the Griffith–Taylor definition for anisotropy; and (3) the presence of (v_6) introduces coupling between the x and y locations. The coupling associated with (v_6) is unique in that it is not present in the extension of the Griffith–Taylor definition [eqn (23)] and furthermore, (v_6) type material coupling cannot be included by studying plate-type theories, which make use of plane stress assumptions. Finally, the shear center location (x^*_{s0}, y^*_{s0}) in the beam root cross-section is determined by solving eqn (26), where (L) is set to zero. An example of the two different "line of shear centers" definitions is presented in Fig. 2, where it is possible that the shear center in the tip cross-section plane can be well outside of the cross-section planform.

COMPUTER PROGRAM

A computer program was written where, first, the boundary of a general cross-section is defined using (n) coordinate points with (n) straight line segments connecting the points. Second, the cross-section is discretized into (n) triangular subregions, where one edge of a triangle is a boundary line segment and the other two edges connect the end-points of a boundary line segment with the user-defined cross-section origin. Thus all of the subregions have one corner that is defined at the origin. Third, the cross-section centroid and principal axes are calculated and then the user-defined cross-section coordinates are transformed to

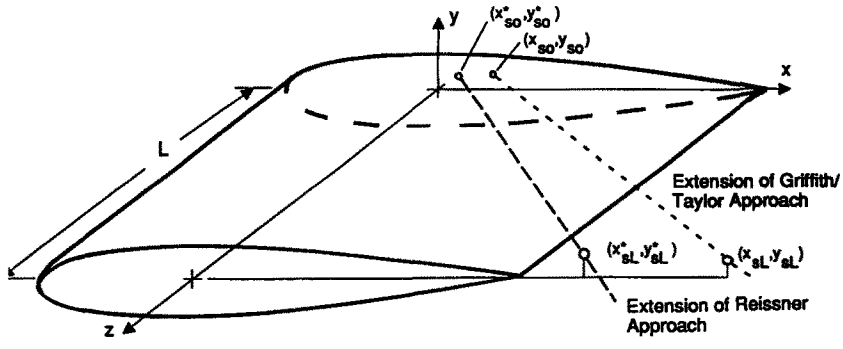

Fig. 2. Line of shear centers in an anisotropic beam.

the cross-section principal axes. Next, the area integrals [eqns (10b–d)] for each triangle subregion are evaluated using exact Gaussian Quadrature formulae (Dunavant, 1985), where the cross-section power series polynomial can be user-defined. Fifth, the complete cross-section stiffness and force matrices are formed by simply adding together (not finite element type assembling) all of the triangular subregion matrices and the three rigid body translations and rigid body rotation are constrained. Sixth, the coefficients for each of the seven cases of $\{Q\}$ are determined. Seventh, the calculated coefficients along with the power series polynomial definition are used to determine the shear stress distribution, the flexibility constants $[a_i(i = 1, \ldots, 7)]$, the cross-section properties (shear center location, torsion constant, shear deformation, etc.) and transform the seven sets of calculated power series coefficients to six sets associated with the six applied loads. Finally, the calculated values are transformed from the principal axes back to the user defined coordinate system.

This approach strongly differs from our previous finite element based approach (Kosmatka and Dong, 1991) in that the global matrix size is defined by the assumed polynomial order and not the complexity of the cross-section. Moreover, cross-section cavities can be easily treated by simply subtracting off the triangular subregions that define the cavity. The aspect ratio of a triangle subregion is not critical, since the power series is a global cross-section function and not a local subregion function (i.e. finite element method).

NUMERICAL RESULTS

Prismatic cantilever beams with three different cross-section types are studied to validate the current approach (ellipse), prove convergence (triangles) and illustrate interesting beam behavior not found in the literature (triangle, NACA-0012 airfoil). See Fig. 3(a–c). Two different materials are considered including an isotropic material (Al 6061-T6, $E = 69$ GPa, $\nu = 0.333$) and a transversely isotropic material [unidirectional high strength graphite/epoxy fibers (Table 1)] with $G_{23} = E_{22}/(2(1+\nu_{23}))$. Generally orthotropic or anisotropic beam behavior is introduced by orienting the material reference frame $(1, 2, 3)$ associated with the graphite/epoxy fibers relative to the beam coordinate frame (x, y, z) using (α) and (β), where the angles are defined in Fig. 4 and the resulting transformation between the two orthonormal coordinate systems is given as

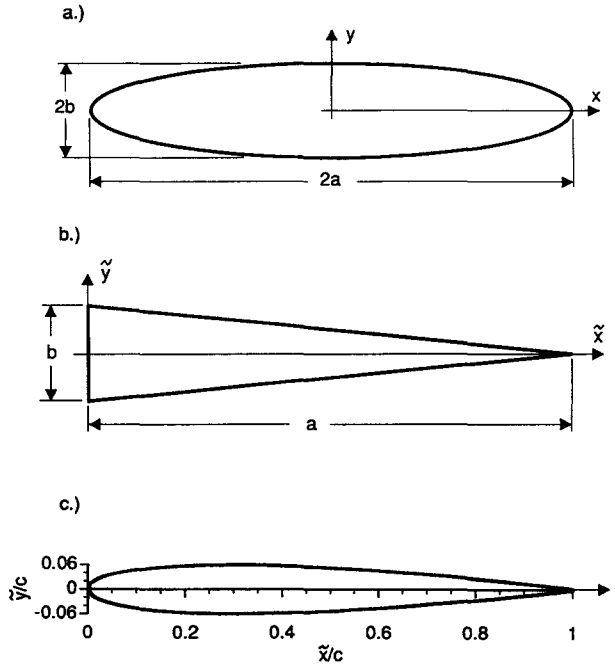

Fig. 3. (a) Elliptical; (b) triangular; and (c) NACA-0012 airfoil cross-sections.

Table 1. Material properties for unidirectional high-strength graphite/epoxy fibers

E_{11}	145 GPa
$E_{22} = E_{33}$	10 GPa
$G_{12} = G_{13}$	4.8 GPa
$\nu_{12} = \nu_{13}$	0.250
ν_{23}	0.400

$$\begin{Bmatrix} 1 \\ 2 \\ 3 \end{Bmatrix} = \begin{bmatrix} \sin(\alpha)\cos(\beta) & \sin(\alpha)\sin(\beta) & \cos(\alpha) \\ \cos(\alpha)\cos(\beta) & \cos(\alpha)\sin(\beta) & -\sin(\alpha) \\ -\sin(\beta) & \cos(\beta) & 0 \end{bmatrix} \begin{Bmatrix} x \\ y \\ z \end{Bmatrix}. \tag{27}$$

The resulting 21 distinct flexibility coefficients (S_{ij}) are determined using standard techniques [see Lekhnitskii (1963)]. Aligning the fiber axes with the beam coordinate axes with ($\alpha = \beta = 0$) will result in transversely isotropic beam behavior with $\nu_4 = \nu_5 = \nu_6 = 0$. Rotating the material axes about the y axis (set $\beta = 0$, and vary α), will produce orthotropic beam behavior with ($\nu_5 \neq 0$) and $\nu_4 = \nu_6 = 0$. Similarly, rotating the material axes about the x axis (set $\beta = 90°$, and vary α), will produce ($\nu_4 \neq 0$, $\nu_5 = \nu_6 = 0$). Finally, rotating the material fibers in the cross-section x–y plane (set $\alpha = 90°$, and vary β) results in ($\nu_4 = \nu_5 = 0$, $\nu_6 \neq 0$).

Elliptical cross-section

The current approach was initially verified by calculating the local cross-section deformations associated with applied flexure (P_y) for anisotropic cantilever beams with elliptical cross-sections having three different aspect ratios ($b/a = 0.1, 1.0, 10.0$) [see Fig. 3(a)] and comparing with the exact local cross-section deformations which can be easily determined by integrating the exact strain distributions given by Lekhnitskii (1963). Anisotropic behavior was introduced by rotating the graphite/epoxy fibers in the x–z plane ($0° < \alpha < 90°$, $\beta = 0°$) so that ν_1, ν_2 and ν_5 are nonzero. Each elliptical cross-section was discretized using 90 points along the perimeter (i.e. divide the cross-section into 90 triangular subregions) and the local deformations of the cross-section (ψ_x, ψ_y, ψ_z) were modeled using cubic polynomials [eqn (7a–d)]. Thus the resulting matrix equation of eqn (10a) had 26

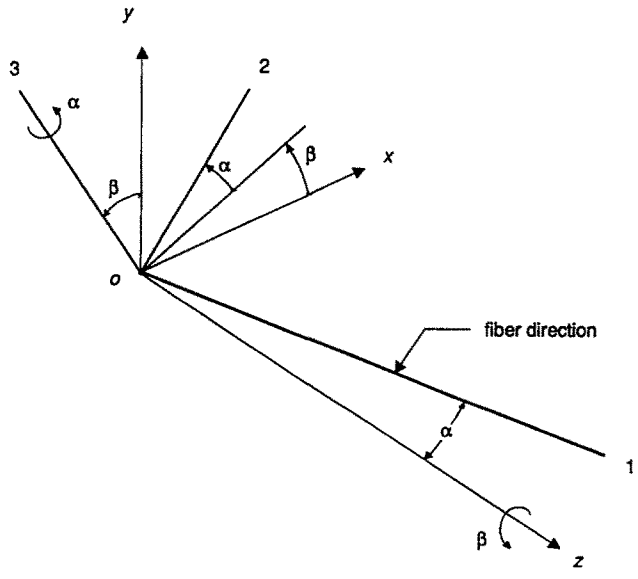

Fig. 4. Orientation of material fibers (1, 2, 3) relative to Cartesian frame (x, y, z).

unknowns. The calculated power series coefficients were found to comprise only nine nonzero values that have the form:

$$\psi_x = P_y(a_{01}y + a_{21}x^2y + a_{03}y^3),$$
$$\psi_y = P_y(b_{10}x + b_{12}xy^2 + b_{30}x^3),$$
$$\psi_z = P_y(c_{01}y + c_{21}x^2y + c_{03}y^3), \tag{28a–c}$$

where these nine coefficients are expressed from eqn (13) as:

$$a_{mn} = (a_{mn(2)} + a_2 a_{mn(7)}),$$
$$b_{mn} = (b_{mn(2)} + a_2 b_{mn(7)}),$$
$$c_{mn} = (c_{mn(2)} + a_2 c_{mn(7)}), \tag{28d–f}$$

and the subscripts (2) and (7) are associated with the second and seventh column of [Ψ]. The remaining 17 coefficients were always identically equal to zero independent of aspect ratio and orientation angle. In Figs 5–7, the variation of the nine nonzero local deformation coefficients is presented as a function of orientation angle (α) for the three aspect ratios, where the exact solutions of Lekhnitskii (1963) are represented by solid lines and the current approach is represented with circles. From these figures it is clear that the current approach can reproduce the exact local deformation result over a broad range of aspect ratios and orientation angles.

Triangular cross-section

A second set of homogeneous isotropic and anisotropic cantilever beams having triangular cross-sections was analysed to first prove convergence of the cross-section parameters with increasing power series polynomial order and second illustrate interesting section property information not found in the literature. The triangle represents an interesting cross-section shape because even though it is geometrically simple (3 corner points,

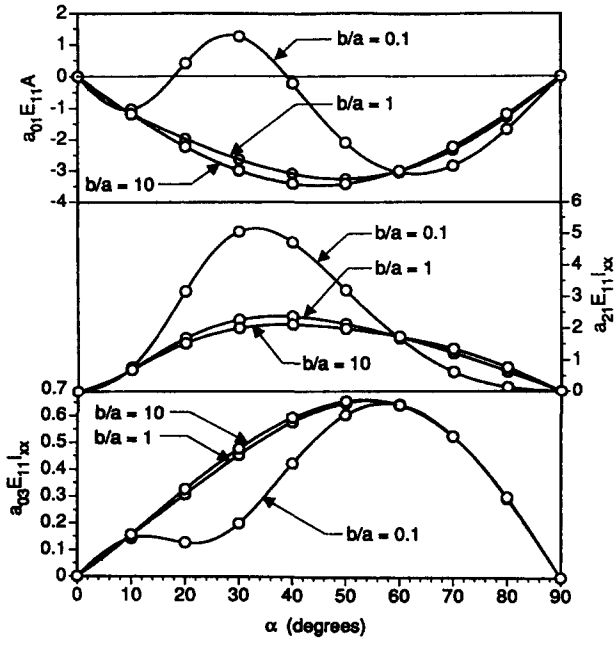

Fig. 5. Nondimensionalized in-plane coefficients (a_{01}, a_{21}, a_{03}) as a function of orientation angle α, ($\beta = 0$) and cross-section aspect ratio b/a for an elliptical cross-section (—— exact, ○ current approach).

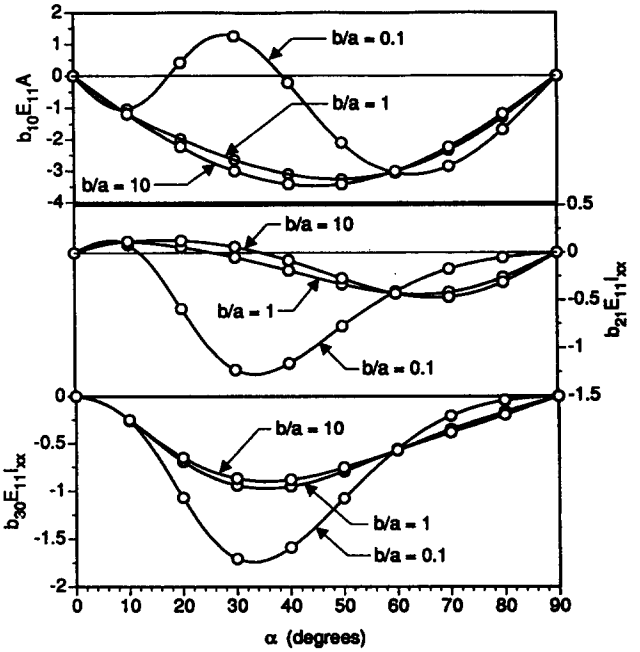

Fig. 6. Nondimensionalized in-plane coefficients (b_{10}, b_{12}, b_{30}) as a function of orientation angle α, ($\beta = 0$) and cross-section aspect ratio b/a for an elliptical cross-section (—— exact, ○ current approach).

three triangular subregions), closed-form torsion and flexure solutions for the local cross-section deformations exist for only the isotropic equilateral triangle, whereas the local cross-section deformations for any other aspect ratio (b/a) are represented by an infinite series of transcendental functions. For these cross-sections, the current approach represents a "best-fit" to the infinite series, where almost all of the calculated coefficients will be nonzero. As the order of the power series polynomial is increased, the calculated coefficients may

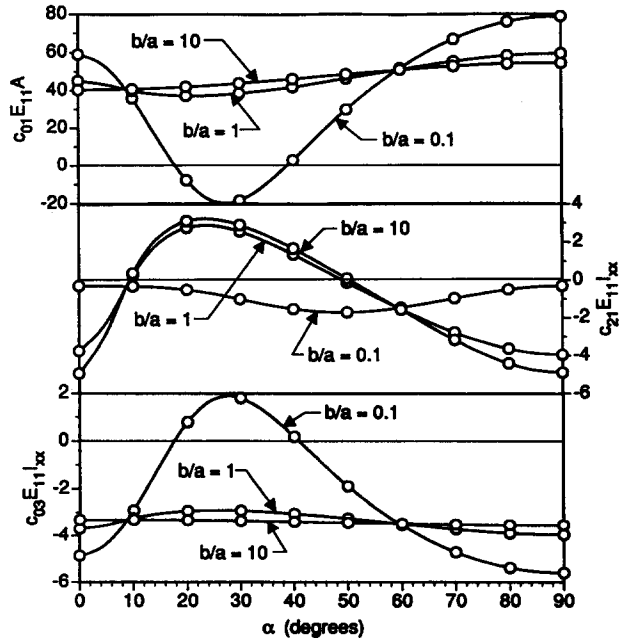

Fig. 7. Nondimensionalized in-plane coefficients (c_{01}, c_{21}, c_{03}) as a function of orientation angle α, ($\beta = 0$) and cross-section aspect ratio b/a for an elliptical cross-section (—— exact, ○ current approach).

vary slightly, but the calculated cross-section integrals (section properties) will experience virtually no change. In this study, a ninth order power-series polynomial was used for each of the three local deformation functions (161 total unknown coefficients) and the numerical integration was performed exactly using a 52-point Gaussian Quadrature formula (Dunavant, 1985). A second coordinate system $(\tilde{x}, \tilde{y})$ is introduced in the triangle [Fig. 3(b)], where the origin is located at the mid-length of the base b and $\tilde{x}$ bisects the triangle.

To study convergence of the section properties with polynomial order, we initially analyse an isotropic (Al 6061-T6) cantilever beam with a thin triangular cross-section ($L/a = 10$, $b/a = 0.1$). In Table 2, the key section parameters are presented as a function of polynomial order and matrix size ($[K]$). The normalized shear center locations, $\tilde{x}_s/a$ and $\tilde{x}_s^*/a$, are presented in the $(\tilde{x}, \tilde{y})$ system, where the two values are significantly different for this thin cross-section, but both approaches exhibit monotonic convergence. The torsion constant ($GJ = 1/a_6$) is also presented, where again the solutions converge quickly. Lastly, the ratios of the centroidal tip displacement associated with shear deformation to the total centroidal tip displacement for applied flexure loads (P_x) and (P_y) are presented, where the magnitudes of the ratios are given, from eqns (17a–c), as:

$$\frac{u_{\text{shear}}}{u_{\text{total}}} = \frac{\gamma_{xz_{(0)}} L}{\gamma_{xz_{(0)}} L + \dfrac{P_x L^3}{3EI_{yy}}}, \qquad \frac{v_{\text{shear}}}{v_{\text{total}}} = \frac{\gamma_{yz_{(0)}} L}{\gamma_{yz_{(0)}} L + \dfrac{P_y L^3}{3EI_{xx}}}. \tag{29a, b}$$

As expected, shear deformation is a much larger effect for flexure loads applied in the x-direction because the effective beam-length aspect ratio is much shorter in the x–z plane ($L/a = 10$) compared to the y–z plane ($L/b = 100$). Both values exhibit monotonic convergence, where it is interesting to note that the x-direction value converges quickly using a low polynomial order (3). A second convergence study was performed using the same geometric beam dimensions, but generally anisotropic behavior was introduced by orientating unidirectional high-stength graphite/epoxy fibers with $\alpha = \beta = 30°$. The calculated section properties are presented as a function of polynomial order in Table 3. The beam root and tip shear center locations are presented using both approaches, where it is observed that: (1) the location converges monotonically with increasing polynomial order; (2) the root shear center locations are within the cross-section; (3) the tip shear center locations are well outside of the cross-section; and (4) the result obtained by extending Reissner's approach is closer to the centroid ($\tilde{x}_s/a = 0.333$), more conservative, than the result obtained by extending the Griffith–Taylor approach. The torsion constant (GJ) and the ratios of the centroidal tip displacement associated with shear deformation to the total centroidal tip displacement for applied flexure loads (P_x) and (P_y) are also presented, where again these parameters converge monotonically.

In addition to the convergence study, three studies are presented that investigate the variation of the shear center location with cross-section aspect ratio and material properties. In Fig. 8, the sensitivity of the shear center location with aspect ratio (b/a) and Poisson's ratio (ν) is presented for an isotropic cantilever beam. The bold solid line and the thin solid lines represent the shear center locations based upon extending Reissner's and Griffith–

Table 2. Calculated section properties of an isotropic cantilever beam with a thin triangular cross-section as a function of power series order ($b/a = 0.1$, $L/a = 10$, $\nu = 0.333$)

Polynomial order	Matrix size	$\tilde{x}_s/a$	$\tilde{x}_s^*/a$	GJ (10^{-3})	$u_{\text{shear}}/u_{\text{total}}$ (10^{-3})	$v_{\text{shear}}/v_{\text{total}}$ (10^{-5})
2	14	0.2718	0.2923	2.168	4.640	−24.26
3	26	0.1398	0.2035	2.118	5.815	4.594
4	41	0.1441	0.2053	2.060	5.815	5.049
5	59	0.1481	0.2070	2.007	5.815	4.583
6	80	0.1515	0.2082	1.969	5.815	4.671
7	104	0.1530	0.2089	1.943	5.815	4.690
8	131	0.1536	0.2093	1.938	5.815	4.700
9	161	0.1536	0.2093	1.936	5.815	4.701

Table 3. Calculated section properties of a generally anisotropic cantilever beam with a thin triangular cross-section as a function of power series order ($b/a = 0.1$, $L/a = 10$, $\alpha = \beta = 30°$)

Polynomial order	$\tilde{x}_{s0}/a$	$\tilde{y}_{s0}/b$ (10^{-2})	$\tilde{x}_{sL}/a$	$\tilde{y}_{sL}/b$	$\tilde{x}^*_{s0}/a$	$\tilde{y}^*_{s0}/b$ (10^{-2})	$\tilde{x}^*_{sL}/a$	$\tilde{y}^*_{sL}/b$	GJ (10^{-4})	u_{shear}/u_{total} (10^{-3})	v_{shear}/v_{total} (10^{-5})
2	0.2724	−0.1881	3.627	0.1434	0.2914	4.231	2.600	−2.246	5.332	5.642	−26.00
3	0.1481	−2.089	3.419	0.1208	0.2049	11.12	2.473	−2.079	5.199	5.468	5.082
4	0.1566	−1.991	3.340	0.1179	0.2099	10.36	2.435	−1.985	5.059	5.461	3.036
5	0.1632	−1.916	3.279	0.1158	0.2137	9.803	2.406	−1.914	4.953	5.469	4.193
6	0.1666	−1.877	3.248	0.1146	0.2159	9.512	2.390	−1.877	4.897	5.475	5.310
7	0.1681	−1.862	3.235	0.1142	0.2166	9.401	2.384	−1.863	4.875	5.475	5.260
8	0.1685	−1.856	3.231	0.1140	0.2169	9.353	2.382	−1.858	4.868	5.474	5.220
9	0.1686	−1.855	3.230	0.1140	0.2170	9.348	2.381	−1.856	4.864	5.474	5.214

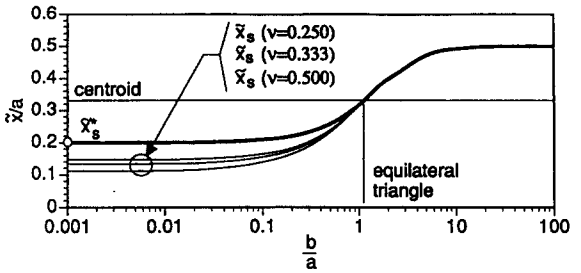

Fig. 8. Variation of the shear center location in an isotropic triangular cross-section as a function of b/a and ν, (—— Griffith–Taylor approach, —— adaption of Reissner approach, ○ Reissner prediction).

Taylor's approaches, respectively, where the shear center location based upon Griffith–Taylor's approach is clearly dependent upon (ν) for thin sections, whereas the extended Reissner-based prediction is independent of (ν). The circular symbol represents the closed form thin-plate prediction of Reissner (1989) for triangular isotropic cross-sections. These results illustrate: (1) for very low aspect ratio triangles the difference in the two approaches for locating the shear center can be profound; (2) the thin plate solutions of Reissner (1989) are valid for only a very small aspect ratio range ($b/a < 0.04$); (3) both shear center predictions converge as the aspect ratio approaches that of an equilateral triangle ($b/a = 1.155$), then ($x_s = x_s^* = 0$); and (4) for large aspect ratios, both shear center predictions are nearly coincident and they converge to the cross-section mid-length ($a/2$). This occurs because for triangular cross-sections with large aspect ratios, the out-of-plane flexural warping function approaches that of a thin rectangle cross-section.

In a second study, the shear center location was determined for a slender cantilever beam ($L/a = 10$) with a thin triangular cross-section ($b/a = 0.01$) composed of off-axis unidirectional high-strength graphite/epoxy fibers ($-90° < \alpha < 90°, \beta = 0°$). In Fig. 9, both shear center locations are presented for the beam root and beam tip as a function of orientation angle (α). At the beam root, the extended Reissner based approach is independent of (α) whereas the extended Griffith–Taylor approach is highly dependent upon (α). This is expected, based upon the above results for an isotropic triangular section which showed that the Griffith–Taylor solution is sensitive to material cross-coupling effects for thin sections. At the beam tip, both approaches for locating the shear center produce identical results when the orientation angle is either close to 0° ($-10° < \alpha < 10°$) or close to 90°

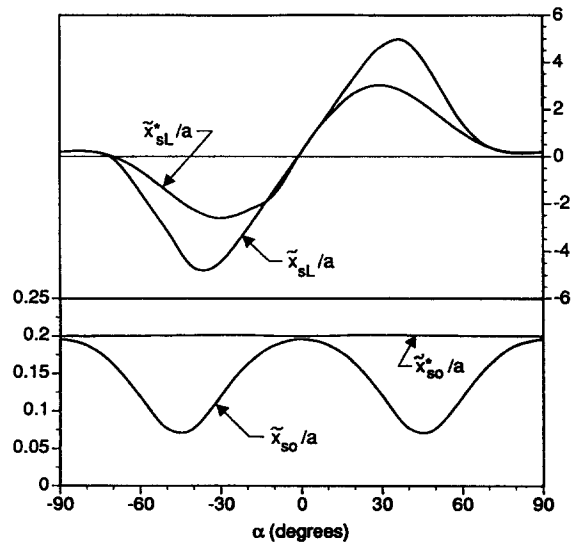

Fig. 9. Variation of the shear center locations at the beam root and beam tip of a thin composite triangular cross-section (b/a) as a function of orientation angle α, ($\beta = 0°$).

$(-70° > \alpha > -110°, 70° < \alpha < 110°)$. Outside of this range, the two approaches produce tip shear center locations that can lie well outside of the cross-section shape, where the extended Reissner approach is much more conservative.

In a third investigation, the sensitivity of the shear center location with varying (v_6) was determined by studying a slender cantilever beam $(L/a = 10)$ with a triangular cross-section $(b/a = 0.1)$ composed of off-axis unidirectional high-strength graphite/epoxy fibers $(\alpha = 0°, -90° < \beta < 90°)$. Since $(v_4 = v_5 = 0)$ the shear center location is a cross-section property that is independent of beam-length. In Fig. 10, both shear center locations are presented as a function of orientation angle (β). In the x-direction, the Griffith–Taylor based prediction is farther from the centroid and more sensitive to (β) than the extended Reissner approach, whereas in the y-direction, the extended Reissner approach is clearly dependent upon (β) and the Griffith–Taylor based prediction is virtually zero.

NACA-0012 cross-section

A final study was performed to investigate the variation of the shear center location with material orientation angle (α) in typical composite general aviation aircraft wings and helicopter blades. These structures are approximated as homogeneous cantilever beams having a NACA-0012 airfoil cross-section [Fig. 3(c)], where a second coordinate system $(\tilde{x}, \tilde{y})$ is introduced with the origin at the leading edge. Two beam-lengths were considered; $(L/c = 3)$ for typical general aviation aircraft wings and $(L/c = 20)$ for long slender helicopter blades, where c is the cross-section chord. The airfoil cross-section is discretized using 95 points on the boundary (i.e. 95 triangular subregions), based upon the mathematical definition of (Abbott and Von Doenhoff, 1959), and the section centroid is located at $(0.42067c)$. Each of the three local deformation functions are modeled using a 9th order power-series polynomial (161 total unknown coefficients) and the numerical integration was performed exactly using a 52-point Gaussian Quadrature formula (Dunavant, 1985).

In Fig. 11, both shear center locations are presented for the beam root and beam tip $(L/c = 3, 20)$ as a function of orientation angle (α). At the beam root the results are similar to the above triangular cross-section study (Fig. 9), where the extended Reissner-based approach is nearly independent of α, whereas the extended Griffith–Taylor approach is slightly more dependent upon α. At the aircraft wing tip (Fig. 11, center region), it is observed that: (1) the two shear center definitions are in near perfect agreement when $(-5° < \alpha < 10°)$ and $(60° < \alpha < 110°)$; (2) the extended Reissner definition of the shear center can be ahead $(\tilde{x} < 0)$ and outside of the airfoil section if $(-8° < \alpha < 52°)$ or behind

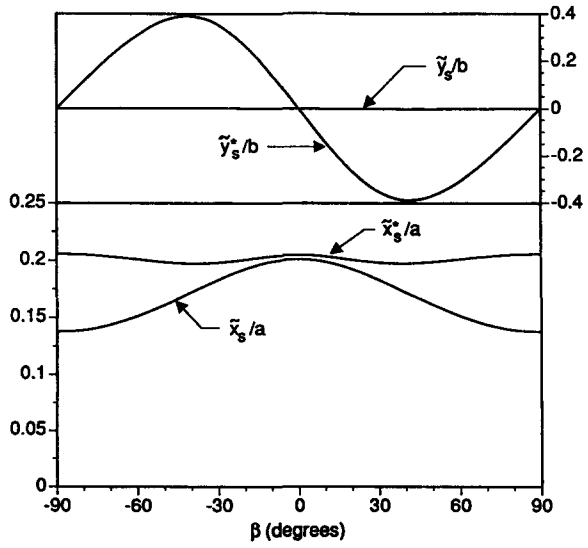

Fig. 10. Variation of the shear center locations at the beam root and beam tip of a thin composite triangular cross-section (b/a) as a function of orientation angle β, $(\alpha = 90°)$.

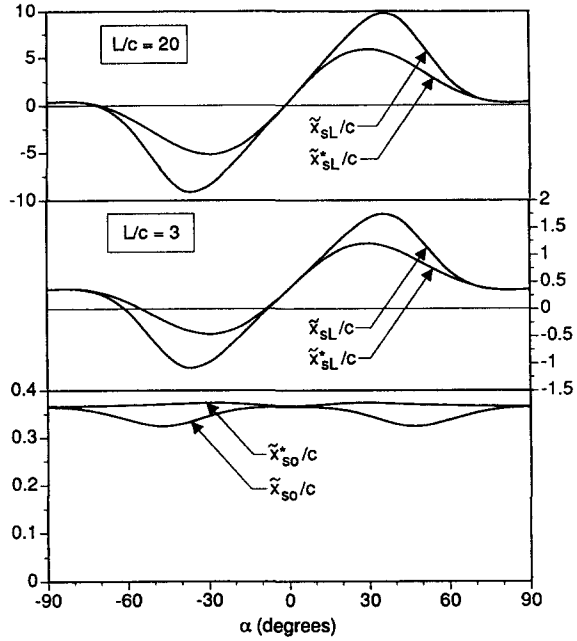

Fig. 11. Variation of the shear center locations at the beam root and beam tip of a composite aircraft ($L/c = 3$) and a composite helicopter blade ($L/c = 20$) as a function of orientation angle α, ($\beta = 0°$).

($\tilde{x} > c$) and outside the airfoil section if ($15° < \alpha < 42°$), whereas the extended Griffith–Taylor definition of the shear center can be ahead ($\tilde{x} < 0$) or behind ($\tilde{x} > c$) the airfoil section if ($-8° < \alpha < -60°$) or ($12° < \alpha < 55°$), respectively; and (3) the maximum distance that the shear center can be located wither ahead or behind the wing-tip section occurs for the extended Reissner definition at ($\alpha = -30°$, $\tilde{x}^*_{sL} = -0.5c$) and ($\alpha = 30°$, $\tilde{x}^*_{sL} = 1.2c$), respectively, whereas the extended Griffith–Taylor definition has ($\alpha = 38°$, $\tilde{x}_{sL} = -1.1c$) and ($\alpha = 36°$, $\tilde{x}_{sL} = 1.7c$), respectively.

For the tip section of the helicopter blade (Fig. 11, upper region), the shape of the curves represent an amplified version of the wing section. Thus, the shear center location is well outside of the tip cross-section for most values of (α), where the maximum distance that the shear center can be located either ahead or behind the wing-tip section occurs for the extended Reissner definition at ($\alpha = 30°$, $\tilde{x}^*_{sL} = -5c$) and ($\alpha = 30°$, $\tilde{x}^*_{sL} = 6.5c$), respectively, whereas the extended Griffith–Taylor definition has ($\alpha = 38°$, $\tilde{x}_{sL} = -9c$) and ($\alpha = 36°$, $\tilde{x}_{sL} = 9c$), respectively.

CONCLUSIONS

The behavior of a tip-loaded anisotropic cantilever beam with an arbitrary cross-section is studied using Saint-Venant's semi-inverse method along with a power series solution for the local in-plane and out-of-plane deformation warping functions. The power series coefficients are determined by solving a set of variationally derived linear algebraic equations. Using the resulting three-dimensional displacement solutions, the shear deformation asssociated with applied tip loads is investigated as well as the shear center location. Two different definitions of the shear center are presented for anisotropic beams by extending the classic approaches of Griffith–Taylor and that of Reissner. Both of the extended definitions reveal the linear dependency of the shear center location with beam-length, where the extended-Reissner prediction is much closer to the centroid then the extended Griffith–Taylor prediction. Numerical results are presented for three different cross-sections and two different materials. For elliptical cross-sections, it was shown that the calculated power series coefficients were in exact agreement with existing elasticity solutions for anisotropic beams over a wide variety of cross-section aspect ratios. For the triangular

cross-sections, it was shown that the calculated power series coefficients represent a "best-fit" to the infinite series of transcendental functions and the warping-related section properties (shear center, torsion constant, shear deformation) converge quickly with increasing power series order. Moreover, three studies were performed to illustrate the sensitivity of the shear center location with cross-section aspect ratio, material definition, fiber orientation, and beam-length. A final investigation was performed to study the length-dependency of the shear center in composite general avaiation aircraft wings ($L/c = 3$) and helicopter blades ($L/c = 20$). At the beam root, the extended Reissner approach is nearly independent of material orientation angle, whereas the extended Griffith–Taylor approach is dependent. At the aircraft wing tip, it is observed that the two shear center definitions are in near perfect agreement over a small range of orientation angles and the shear center can be located either ahead or behind the wing-tip section. For the helicopter blade tip section, the shear center location is well outside of the tip cross-section for most values of orientation angle.

Acknowledgements—The support of this research was provided by the NASA-Langley Research Center through grant NAG-1-1151-FDP, with R. C. Lake as project monitor.

REFERENCES

Abbott, I. R. and Von Doenhoff, A. E. (1959). *Theory of Wing Sections*. Dover, New York.

Dunavant, D. A. (1985). High degree efficient symmetrical Gaussian quadrature rules for triangle. *Int. J. Numer. Meth. Engng* **21,** 1129–1148.

Griffith, A. A. and Taylor, G. I. (1917). The problem of flexure and its solution by the soap-film method. Reports and Memoranda Adv. Comm. Aeronautics, No. 399.

Herrmann, L. R. (1965). Elastic torsional analysis of irregular shapes. *J. Engng Mech. Div. ASCE* **91**(EM6), 11–19.

Kosmatka, J. B. (1986). Structural dynamic modeling of advanced composite propellers by the finite element method. Ph.D. Dissertation, University of California, Los Angles.

Kosmatka, J. B. (1992). Flexture-torsion behavior of prismatic beams. Part I: Section properties via power series. *AIAA Jl* **31**(1), 170–179.

Kosmatka, J. B. and Dong, S. B. (1991). Saint-Venant solution for prismatic anisotropic beams. *Int. J. Solids Structures* **28,** 917–938.

Lekhnitskii, S. G. (1963). *Theory of Elasticity of an Anisotropic Body*. Holden-Day, San Francisco.

Libove, C. (1988). Stresses and rate of twist in single-cell thin-walled beams with anisotropic walls. *AIAA Jl* **26**(9), 1107–1118.

Mason, W. E. and Herrmann, L. R. (1968). Elastic shear analysis of general prismatic shaped beams. *J. Engng Mech. Div. ASCE* **94**(EM4), 965–983.

Mindlin, R. D. (1975). Solution of St. Venant's torsion problem by power series. *Int. J. Solids Structures* **11,** 321–328.

Reissner, E. (1989). The center of shear as a problem of the theory of plates of variable thickness. *Ing.-Archiv.* **59,** 324–332.

Reissner, E. (1991). Approximate determinations of the center of shear by use of the Saint-Venant solution for the flexure problem of plates of variable thickness. *Arch. Appl. Mech.-Ing.-Archiv.* **61,** 555–566.

Sokolnikoff, I. S. (1946). *Mathematical Theory of Elasticity*. McGraw-Hill, New York.

APPENDIX

The matrix $[\overline{F_C}]$ is defined as:

$$[\overline{F_C}] = \begin{bmatrix} -\frac{v_1}{EI_{yy}}x(z-L) & -\frac{v_1}{EI_{xx}}y(z-L) & 0 & 0 & 0 & 0 & 0 \\ -\frac{v_2}{EI_{yy}}x(z-L) & -\frac{v_2}{EI_{xx}}y(z-L) & 0 & 0 & 0 & 0 & 0 \\ -\frac{1}{2EI_{yy}}\{v_5x+v_4y-2(z-L)\}x-\frac{v_5}{2EA} & -\frac{1}{2EI_{xx}}\{v_5x+v_4y-2(z-L)\}y-\frac{v_4}{2EA} & \frac{1}{EA} & \frac{1}{EI_{xx}}y & -\frac{1}{EI_{yy}}x & \frac{v_5}{2EI_{xx}}y-\frac{v_4}{2EI_{yy}}x & 0 \\ -\frac{1}{EI_{yy}}\left\{\frac{v_6}{2}x+v_2y+v_4(z-L)\right\}x & \frac{1}{2EI_{xx}}\{(v_1x^2-v_2y^2)-2v_4y(z-L)\} & 0 & 0 & 0 & 0 & x \\ -\frac{1}{2EI_{yy}}\{(v_1x^2-v_2y^2)+2v_5x(z-L)\} & -\frac{1}{EI_{xx}}\left\{v_1x+\frac{v_6}{2}y+v_5(z-L)\right\}y & 0 & 0 & 0 & 0 & -y \\ -\frac{v_6}{EI_{yy}}x(z-L) & -\frac{v_6}{EI_{xx}}y(z-L) & 0 & 0 & 0 & 0 & 0 \end{bmatrix}. \quad \text{(A1)}$$

Integrating the matrix (A1) over the beam length results in

$$\int_0^L [\overline{F_C}]\,dz = L[\overline{\overline{F_C}}], \tag{A2}$$

where

$$[\overline{\overline{F_C}}] = \begin{bmatrix} \frac{v_1 L}{2EI_{yy}}x & \frac{v_1 L}{2EI_{xx}}y & 0 & 0 & 0 & 0 & 0 \\ \frac{v_2 L}{2EI_{yy}}x & \frac{v_2 L}{2EI_{xx}}y & 0 & 0 & 0 & 0 & 0 \\ -\frac{1}{2EI_{yy}}\{v_5 x+v_4 y+L\}x-\frac{v_5}{2EA} & -\frac{1}{2EI_{xx}}\{v_5 x+v_4 y+L\}y-\frac{v_4}{2EA} & \frac{1}{EA} & \frac{1}{EI_{xx}}y & -\frac{1}{EI_{yy}}x & \frac{v_5}{2EI_{xx}}y-\frac{v_4}{2EI_{yy}}x & 0 \\ -\frac{1}{2EI_{yy}}\{v_6 x+2v_2 y-v_4 L\}x & \frac{1}{2EI_{xx}}\{(v_1 x^2-v_2 y^2)+v_4 Ly\} & 0 & 0 & 0 & 0 & x \\ -\frac{1}{2EI_{yy}}\{(v_1 x^2-v_2 y^2)-v_5 Lx\} & -\frac{1}{2EI_{xx}}\{2v_1 x+v_6 y-v_5 L\}y & 0 & 0 & 0 & 0 & -y \\ \frac{v_6 L}{2EI_{yy}}x & \frac{v_6 L}{2EI_{xx}}y & 0 & 0 & 0 & 0 & 0 \end{bmatrix}. \tag{A3}$$